

Phenomenology of $B \rightarrow \pi\pi, \pi K$ Decays at $\mathcal{O}(\alpha_s^2\beta_0)$ in QCD Factorization

Craig N. Burrell

*Department of Physics, University of Toronto
60 St. George Street, Toronto, Ontario, Canada M5S 1A7**

Alexander R. Williamson

*Department of Physics, Carnegie Mellon University,
Pittsburgh, PA 15213[†]*

We study $\mathcal{O}(\alpha_s^2\beta_0)$ perturbative corrections to matrix elements entering two-body exclusive decays of the form $\bar{B} \rightarrow \pi\pi, \pi K$ in the QCD factorization formalism, including chirally enhanced power corrections, and discuss the effect of these corrections on direct CP asymmetries, which receive their first contribution at $\mathcal{O}(\alpha_s)$. We find that the $\mathcal{O}(\alpha_s^2\beta_0)$ corrections are often as large as the $\mathcal{O}(\alpha_s)$ corrections. We find large uncertainties due to renormalization scale dependence as well as poor knowledge of the non-perturbative parameters. We assess the effect of the perturbative corrections on the direct CP violation parameters of $B^0 \rightarrow \pi^+\pi^-$.

*Electronic address: craig.burrell@utoronto.ca

[†]Electronic address: alexwill@andrew.cmu.edu

I. INTRODUCTION

In recent years a wealth of new data on two-body nonleptonic B decays to light pseudoscalar final states has been produced by the CLEO [1, 2, 3], BABAR [4, 5, 6, 7, 8, 9, 10, 11, 12] and BELLE [13, 14, 15, 16, 17] experiments. This experimental program provides a rich context for the precision study of the weak sector of the standard model. However, in non-leptonic decays all of the final state particles are QCD bound states which interact strongly with one another. There is therefore nonperturbative physics in the low energy matrix elements which is an obstacle to precision calculations.

These low energy matrix elements can be evaluated if it is assumed that they factorize into simpler matrix elements [18]. For example,

$$\langle \pi^+ K^- | (\bar{u}b)_{V-A} (\bar{s}u)_{V-A} | \bar{B} \rangle \rightarrow \langle K^- | (\bar{s}u)_{V-A} | 0 \rangle \langle \pi^+ | (\bar{u}b)_{V-A} | \bar{B} \rangle. \quad (1)$$

The matrix elements on the right-hand side can be parametrized in terms of form factors and decay constants. This ‘naive factorization’ prescription has in some cases proven to be a remarkably successful approximation [19, 20, 21]. As it stands, however, there is no way to improve the calculation by making systematic corrections in a controlled expansion. Moreover, the missing ‘non-factorizable’ physics is responsible for final-state rescattering and strong interaction phase shifts, and is therefore of considerable interest.

Beneke, Buchalla, Neubert, and Sachrajda (BBNS) [22, 23, 24] have argued that for certain classes of two-body nonleptonic B decays the strong interactions which break factorization are perturbative in the heavy quark limit [22, 23]. The physical picture behind this claim is ‘color transparency’: gluons must be energetic to resolve the small color dipole structure of the energetic light meson in the final state. The BBNS proposal, called QCD factorization, was accompanied by a demonstration that, for heavy-light final states, it holds up to two-loop order [23] in the heavy quark limit. This conclusion was subsequently extended to all orders in perturbation theory [25, 26].

The BBNS proposal reproduces naive factorization as the leading term in an expansion in α_s and Λ_{QCD}/m_b , thereby placing naive factorization on a more secure theoretical foundation. Although there has been some recent progress [27, 28, 29, 30, 31, 32, 33], at present there exists no systematic way to address the Λ_{QCD}/m_b corrections. The perturbative corrections, on the other hand, can be calculated, and the $\mathcal{O}(\alpha_s)$ corrections are known for a variety of decay modes [22, 23, 24, 34, 35, 36].

In this paper we study $\mathcal{O}(\alpha_s^2 \beta_0)$ perturbative corrections to B decays of the form $B \rightarrow \pi\pi, \pi K$. Though this is only a subset of the full $\mathcal{O}(\alpha_s^2)$ correction, the method is motivated by the empirical observation that the $\mathcal{O}(\alpha_s^2 \beta_0)$ contribution often dominates the full result. For example, this is true for $R(e^+e^- \rightarrow \text{hadrons})$ [37], $\Gamma(\tau \rightarrow \nu_\tau + \text{hadrons})$ [38], and $\Gamma(b \rightarrow X_u e \bar{\nu}_e)$ [39]. The dominance of the $\mathcal{O}(\alpha_s^2 \beta_0)$ contribution becomes rigorous in the very formal ‘large- β_0 limit’ of QCD, where the number of colors is fixed and the number of flavours $n_f \rightarrow -\infty$, resulting in $\beta_0 = 11 - 2/3n_f \rightarrow \infty$.

The perturbative corrections we consider arise from three sources: ‘non-factorizable’ vertex corrections, QCD penguin diagrams, and spectator quark interactions. In the BBNS framework the computation of these amplitudes requires the introduction of a number of nonperturbative parameters. We study the numerical significance of the uncertainties due to these parameters. We neglect power corrections of the form $\mathcal{O}(\Lambda_{\text{QCD}}/m_b)^n$, with the exception of a class of ‘chirally enhanced’ corrections that can be numerically significant. Renormalon studies of these decays indicate that the leading power corrections from soft gluons are at $\mathcal{O}(\Lambda_{\text{QCD}}/m_b)$ [40]. This is in contrast to $B \rightarrow D\pi$ decays where a similar analysis points to leading power corrections at $\mathcal{O}(\Lambda_{\text{QCD}}/m_b)^2$ [41, 42].

The calculations presented in this paper are similar to calculations performed earlier by Neubert and Pecjak in [40], although they differ in several important ways. The goal of the previous paper was to study power corrections to $B \rightarrow LL$ decays in a manner similar to what had been done for $B \rightarrow D^{(*)}L$ decays in [41, 42]. The authors calculated the amplitudes to $\mathcal{O}(1/\beta_0)$, which is subleading in the large- β_0 limit. With these expressions they derived predictions for the CP asymmetries of several decay modes. The calculation involved summing a class of graphs to all orders in perturbation theory, and extracting from their large order perturbative behaviour information about power corrections. Estimates of the $\mathcal{O}(\alpha_s^n \beta_0^{n-1})$ corrections were also made in the large- β_0 limit.

Our focus is the convergence behaviour of perturbation theory in the BBNS framework. Instead of calculating to subleading order in the large- β_0 limit, we restrict ourselves to $\mathcal{O}(\alpha_s^2 \beta_0)$ corrections. To avoid the need for Wilson coefficients evaluated at NNLO, we concentrate on observables which vanish at leading order in perturbation theory. In particular, we study the direct CP asymmetries for six pseudo-scalar final states $\mathcal{A}_{\text{CP}}^{\text{Dir}}(\pi\pi, \pi K)$. Though several of these modes also exhibit indirect CP violation, we restrict our discussion to direct CP violation only. We find that the $\mathcal{O}(\alpha_s^2 \beta_0)$ corrections are similar in size to the $\mathcal{O}(\alpha_s)$ values. We also find that the greatest uncertainty in the CP asymmetries is due to the renormalization scale dependence, which is enhanced by the $\mathcal{O}(\alpha_s^2 \beta_0)$ corrections. In contrast, the uncertainties induced in the asymmetries by nonperturbative parameters are relatively small. Of particular interest is the mode $\mathcal{A}_{\text{CP}}^{\text{Dir}}(\pi^- \bar{K}^0)$ which, to the order we work, is independent of most of the nonperturbative parameters in the analysis.

At the end of the paper we present a more detailed analysis of the direct asymmetry parameter $\mathcal{A}_{\pi\pi}$, which has attracted considerable interest recently [8, 15]. We find that this parameter receives a substantial correction at $\mathcal{O}(\alpha_s^2 \beta_0)$, the size of which we give as a function of the unitarity angle γ . We examine the relationship between this quantity and the current experimental values, and find them to be in agreement within the large theoretical and experimental uncertainties.

The structure of this paper is as follows: in the first Section we briefly review the theoretical context for our calculation; in the subsequent Section we give an outline of our method and collect most of our analytical results. This is followed by a brief phenomenological study of direct CP asymmetries for a variety of different decays to $\pi\pi, \pi K$ final states, pay-

ing special attention to the $\mathcal{O}(\alpha_s^2\beta_0)$ corrections. In the concluding Section we summarize our results.

II. THEORETICAL BACKGROUND

We work in the weak effective theory where the weak bosons and top quark have been integrated out. The effective Hamiltonian, valid below M_W , is

$$\mathcal{H}_{\text{eff}} = \frac{G_F}{\sqrt{2}} \sum_{p=u,c} \lambda_p^{(\prime)} \left(C_1 \mathcal{O}_1^p + C_2 \mathcal{O}_2^p + \sum_{i=3,\dots,6} C_i \mathcal{O}_i + C_{8g} \mathcal{O}_{8g} \right) + h.c. \quad (2)$$

where the CKM matrix elements are $\lambda_p = V_{ps}^* V_{pb}$ for the $\Delta S = 1$ Hamiltonian and $\lambda_p' = V_{pd}^* V_{pb}$ for decays to non-strange final states. The effective operators mediating the decays are divided into left-handed current-current operators ($\mathcal{O}_{1,2}^p$), QCD penguin operators ($\mathcal{O}_{3,\dots,6}$), and a chromomagnetic dipole operator (\mathcal{O}_{8g}). Explicitly, the operator basis for the $\Delta S = 1$ Hamiltonian is [43]

$$\begin{aligned} \mathcal{O}_1^p &= (\bar{p}b)_{V-A} (\bar{s}p)_{V-A}, & \mathcal{O}_2^p &= (\bar{p}_i b_j)_{V-A} (\bar{s}_j p_i)_{V-A}, \\ \mathcal{O}_3 &= (\bar{s}b)_{V-A} \sum_q (\bar{q}q)_{V-A}, & \mathcal{O}_4 &= (\bar{s}_i b_j)_{V-A} \sum_q (\bar{q}_j q_i)_{V-A}, \\ \mathcal{O}_5 &= (\bar{s}b)_{V-A} \sum_q (\bar{q}q)_{V+A}, & \mathcal{O}_6 &= (\bar{s}_i b_j)_{V-A} \sum_q (\bar{q}_j q_i)_{V+A}, \\ \mathcal{O}_{8g} &= \frac{-g_s}{8\pi^2} m_b \bar{s} \sigma_{\mu\nu} (1 + \gamma_5) G^{\mu\nu} b. \end{aligned} \quad (3)$$

The $\Delta S = 0$ operator set is as above with the s fields replaced by d fields. In these expressions we use the shorthand $(\bar{q}q')_{V\pm A} = \bar{q}\gamma^\mu(1\pm\gamma_5)q'$ for the Dirac structures. Roman indices on quark fields denote $SU(3)$ color structure, and the summations over q in the penguin operators \mathcal{O}_{3-6} run over all five active quark flavours $q \in \{d, u, s, c, b\}$. Some authors include in (3) a set of electroweak penguin operators which, however, produce only small effects and are neglected in our analysis. The values of the Wilson coefficients $C_i(\mu)$ are obtained by matching the effective theory onto the full theory at $\mu = m_W$ and running down to $\mu \sim m_b$. This procedure has been carried out to NLO in QCD, the results of which can be found in [43].

The low energy dynamics are contained in the matrix elements of the four-quark operators \mathcal{O}_i . In the BBNS framework these matrix elements are given by

$$\begin{aligned} \langle M_1 M_2 | \mathcal{O} | \bar{B} \rangle &= F^{B \rightarrow M_1} (m_{M_2}^2) f_{M_2} \int_0^1 dx T^I(x) \Phi_{M_2}(x) + (M_1 \leftrightarrow M_2) \\ &+ \int_0^1 dx dy d\xi T^{II}(x, y, \xi) \Phi_{M_1}(y) \Phi_{M_2}(x) \Phi_B(\xi) + \mathcal{O}\left(\frac{\Lambda_{\text{QCD}}}{m_b}\right). \end{aligned} \quad (4)$$

where M_1 is the meson which receives the spectator quark of the B meson and M_2 is called the ‘emission meson’. The nonperturbative elements in this expression are the B decay form factors $F^{B \rightarrow M}$, the final state meson decay constants f_M , and the light-cone momentum

distribution amplitudes Φ_M , which give the probability for a valence quark to carry a particular fraction of the meson's light-cone momentum. The quark and antiquark composing the emission meson M_2 are assigned momentum fractions x and \bar{x} , respectively. Likewise the quark and antiquark in M_1 are assigned momentum fractions y and \bar{y} , respectively. The light antiquark in the B meson is assigned momentum fraction ξ of the B meson momentum. In the heavy quark limit, we can neglect components of momentum transverse to the light cone, and consider only the Fock state containing the valence quark and antiquark. Thus we have $\bar{x} = 1 - x$, and likewise for y and ξ .

The factorization-breaking corrections are contained in the hard-scattering kernels $T^I(x)$ and $T^{II}(x, y, \xi)$, each of which has a perturbative expansion. At leading order, the hard-scattering kernels take the values [22, 23, 44]

$$T^I(x) = 1 + \mathcal{O}(\alpha_s); \quad T^{II}(x, y, \xi) = 0 + \mathcal{O}(\alpha_s) \quad (5)$$

and, given that the light-cone wavefunctions Φ_{M_i} are normalized to unity, (4) reduces to naive factorization.

The nonperturbative light-cone distribution amplitudes (LCDAs) Φ_M in (4) are defined by [45, 46]

$$\langle P(p) | \bar{q}_\beta(z_2) q_\alpha(z_1) | 0 \rangle = \quad (6)$$

$$i \frac{f_P}{4} \int_0^1 dx e^{i(x p \cdot z_2 + \bar{x} p \cdot z_1)} \left[\not{p} \gamma_5 \Phi(x) - \mu_P \gamma_5 \left(\Phi_p(x) - \sigma^{\mu\nu} p_\mu (z_2 - z_1)_\nu \frac{\Phi_\sigma(x)}{6} \right) \right]_{\alpha\beta}.$$

In this equation $\Phi(x)$ is the meson twist-2 LCDA, and $\Phi_{p,\sigma}(x)$ are twist-3 LCDAs which will contribute to the ‘chirally enhanced’ power corrections below. The quantity μ_P appearing in (6) is a ‘chiral enhancement’ factor

$$\mu_P = \frac{m_P^2}{m_q + m_{\bar{q}}} \quad (7)$$

where q and \bar{q} are the quarks which comprise the valence state of the pseudoscalar meson P . In practice one introduces these LCDAs into Feynman amplitudes by replacing quark bilinears with a projection matrix M [24]

$$\bar{u}_{\beta,a}(xp) \Gamma_{\beta\alpha,ab} v_{\alpha,b}(\bar{x}p) \rightarrow \frac{if_P}{4N_c} \int_0^1 dx M_{\alpha\beta}^P \Gamma_{\beta\alpha,aa} \quad (8)$$

where

$$M^P = \not{p} \gamma_5 \Phi(x) - \mu_P \gamma_5 \frac{\not{p}_2 \not{p}_1}{p_1 \cdot p_2} \Phi_p(x). \quad (9)$$

In these expressions Greek indices denote Dirac structure, Roman indices denote color structure, and Γ is an arbitrary combination of Dirac and color matrices. The momenta $p_{1,2}$ are the momenta of the meson quark and antiquark, respectively. In the collinear limit $p_1 = xp$ and $p_2 = \bar{x}p$. In order to arrive at (9) from the definition (6) the equations of motion for the twist-3 LCDAs and an integration by parts have been used to eliminate Φ_σ [24, 47].

Throughout this paper we write the twist-2 LCDAs as a decomposition over Gegenbauer polynomials as [48]

$$\Phi_M(x) = 6x(1-x) \left[1 + \sum_{n=1}^{\infty} \alpha_n^M(\mu) C_n^{3/2}(2x-1) \right] \quad (10)$$

where the Gegenbauer polynomials $C_n^{3/2}(y)$ are defined by the generating function

$$C_n^{3/2}(y) = \frac{1}{n!} \frac{d^n}{dh^n} (1-2hy+h^2)^{-3/2} \Big|_{h=0}. \quad (11)$$

The Gegenbauer moments α_i^M have been studied using nonperturbative methods in QCD and, for many light mesons, estimates exist for the leading moments $\alpha_{1,2}^M$ [45, 49, 50]. In the far ultraviolet $\mu \rightarrow \infty$ we have $\alpha_i^M \rightarrow 0$, so at the scale $\mu \sim m_b$, which is still large compared to the nonperturbative scale of QCD, the Gegenbauer moments α_i^M are expected to be small. This statement will be made more quantitative in Section IV. In the approximation of including only ‘chirally enhanced’ twist-3 contributions, the twist-3 LCDA equations of motion constrain $\Phi_p(x)$ to take its asymptotic form $\Phi_p(x) = 1$ [24].

Following the authors of [24] we use the factorization formula (4) to rewrite matrix elements of (2) in the convenient form

$$\langle \pi K | \mathcal{H}_{\text{eff}} | \bar{B} \rangle = \frac{G_F}{\sqrt{2}} \sum_{p=u,c} \lambda_p \langle \pi K | \mathcal{T}_p | \bar{B} \rangle, \quad (12)$$

where

$$\begin{aligned} \mathcal{T}_p = & a_1 \delta_{pu} (\bar{u}b)_{V-A} \otimes (\bar{s}u)_{V-A} \\ & + a_2 \delta_{pu} (\bar{s}b)_{V-A} \otimes (\bar{u}u)_{V-A} \\ & + a_3 \sum_q (\bar{s}b)_{V-A} \otimes (\bar{q}q)_{V-A} \\ & + a_4^p \sum_q (\bar{q}b)_{V-A} \otimes (\bar{s}q)_{V-A} \\ & + a_5 \sum_q (\bar{s}b)_{V-A} \otimes (\bar{q}q)_{V+A} \\ & + a_6^p \sum_q (-2) (\bar{q}b)_{S-P} \otimes (\bar{s}q)_{S+P} \end{aligned} \quad (13)$$

where $(\bar{q}q')_{S\pm P} = \bar{q}(1 \pm \gamma_5)q'$, and a summation over $q \in \{u, d\}$ is implied. There is a similar expression for $\pi\pi$ final states, obtained by replacing the s quark by a d quark. Matrix elements of operators containing the \otimes product are to be evaluated as one would in naive factorization

$$\langle M_1 M_2 | j_1 \otimes j_2 | B \rangle \equiv \langle M_1 | j_1 | B \rangle \langle M_2 | j_2 | 0 \rangle \text{ or } \langle M_2 | j_1 | B \rangle \langle M_1 | j_2 | 0 \rangle \quad (14)$$

where the choice depends on the specific quark content of the mesons in the process under consideration. The nonfactorizable corrections are contained in the coefficients a_i . Though we have not explicitly indicated it in (13), in general these coefficients are mode specific, dependent on the shapes of the LCDAs of the final state particles. We present the explicit forms for a_i in section III.

III. PERTURBATIVE CORRECTIONS

We consider three classes of diagrams: factorization-breaking vertex diagrams, strong interactions with the initial state spectator quark, and QCD penguin diagrams. They are shown in Figures 2 – 4. The first and third of these classes contribute to the hard scattering kernel T^I in (4); the second contributes to T^{II} . In this paper we do not include the power suppressed weak annihilation diagrams which have been studied by other authors [24].

The diagrams at $\mathcal{O}(\alpha_s^2\beta_0)$ are obtained by replacing the gluon in the $\mathcal{O}(\alpha_s)$ diagram by a gluon with a fermion–loop self–energy correction, as shown in Figure 1, followed by the replacement $n_f \rightarrow -3\beta_0/2$.

$$\alpha_s: \quad \text{---} \text{---} \text{---} \text{---} \text{---} = \text{---} \text{---} \text{---}$$

$$\alpha_s^2 \beta_0: \quad \text{---} \text{---} \text{---} \text{---} \text{---} = \text{---} \text{---} \text{---} \text{---} \text{---}$$

FIG. 1: The form of the dashed gluon line in Figures 2 – 4 at each order in perturbation theory. Where an undressed gluon line provides the $\mathcal{O}(\alpha_s)$ contribution, the fermion–loop self–energy correction produces the $\mathcal{O}(\alpha_s^2\beta_0)$ contributions.

All of the perturbative corrections are contained in the coefficients a_i defined in (13). These coefficients may be written as

$$a_1 = C_1 + \frac{C_2}{N_c} \left[1 + C_F \left\{ \frac{\alpha_s(\mu)}{4\pi} V_{M_2} + \left(\frac{\alpha_s(\mu)}{4\pi} \right)^2 \beta_0 \tilde{V}_{M_2} \right\} \right. \\ \left. + \frac{4C_F\pi^2}{N_c} \left\{ \frac{\alpha_s(\mu_h)}{4\pi} H_{M_2M_1} + \left(\frac{\alpha_s(\mu_h)}{4\pi} \right)^2 \beta_0 \tilde{H}_{M_2M_1} \right\} \right],$$

$$a_2 = C_2 + \frac{C_1}{N_c} \left[1 + C_F \left\{ \frac{\alpha_s(\mu)}{4\pi} V_{M_2} + \left(\frac{\alpha_s(\mu)}{4\pi} \right)^2 \beta_0 \tilde{V}_{M_2} \right\} \right. \\ \left. + \frac{4C_F\pi^2}{N_c} \left\{ \frac{\alpha_s(\mu_h)}{4\pi} H_{M_2M_1} + \left(\frac{\alpha_s(\mu_h)}{4\pi} \right)^2 \beta_0 \tilde{H}_{M_2M_1} \right\} \right],$$

$$a_3 = C_3 + \frac{C_4}{N_c} \left[1 + C_F \left\{ \frac{\alpha_s(\mu)}{4\pi} V_{M_2} + \left(\frac{\alpha_s(\mu)}{4\pi} \right)^2 \beta_0 \tilde{V}_{M_2} \right\} \right. \\ \left. + \frac{4C_F\pi^2}{N_c} \left\{ \frac{\alpha_s(\mu_h)}{4\pi} H_{M_2M_1} + \left(\frac{\alpha_s(\mu_h)}{4\pi} \right)^2 \beta_0 \tilde{H}_{M_2M_1} \right\} \right],$$

$$a_4^p = C_4 + \frac{C_3}{N_c} \left[1 + C_F \left\{ \frac{\alpha_s(\mu)}{4\pi} V_{M_2} + \left(\frac{\alpha_s(\mu)}{4\pi} \right)^2 \beta_0 \tilde{V}_{M_2} \right\} \right. \\ \left. + \frac{4C_F\pi^2}{N_c} \left\{ \frac{\alpha_s(\mu_h)}{4\pi} H_{M_2M_1} + \left(\frac{\alpha_s(\mu_h)}{4\pi} \right)^2 \beta_0 \tilde{H}_{M_2M_1} \right\} \right]$$

$$\begin{aligned}
& + \frac{C_F}{N_c} \left\{ \frac{\alpha_s(\mu)}{4\pi} P_{M_2,2}^p + \left(\frac{\alpha_s(\mu)}{4\pi} \right)^2 \beta_0 \tilde{P}_{M_2,2}^p \right\}, \\
a_5 = & C_5 + \frac{C_6}{N_c} \left[1 - C_F \left\{ \frac{\alpha_s(\mu)}{4\pi} V'_{M_2} + \left(\frac{\alpha_s(\mu)}{4\pi} \right)^2 \beta_0 \tilde{V}'_{M_2} \right\} \right. \\
& \left. - \frac{4C_F\pi^2}{N_c} \left\{ \frac{\alpha_s(\mu_h)}{4\pi} H'_{M_2M_1} + \left(\frac{\alpha_s(\mu_h)}{4\pi} \right)^2 \beta_0 \tilde{H}'_{M_2M_1} \right\} \right], \\
a_6^p = & C_6 + \frac{C_5}{N_c} \left[1 + C_F \left\{ \frac{\alpha_s(\mu)}{4\pi} (-6) + \left(\frac{\alpha_s(\mu)}{4\pi} \right)^2 \beta_0 (-4) \right\} \right] \\
& + \frac{C_F}{N_c} \left\{ \frac{\alpha_s(\mu)}{4\pi} P_{M_2,3}^p + \left(\frac{\alpha_s(\mu)}{4\pi} \right)^2 \beta_0 \tilde{P}_{M_2,3}^p \right\}, \tag{15}
\end{aligned}$$

where $C_i \equiv C_i(\mu)$. The nonperturbative physics is contained in the functions labelled V, H , and P , according to the type of diagram from which they arise. In particular, the non-factorizable vertex corrections, treated in section III A below, produce the functions $V_M^{(\prime)}$ and $\tilde{V}_M^{(\prime)}$. The scattering of hard gluons off the spectator quark, treated in section III B, gives rise to the functions $H_{M_2M_1}^{(\prime)}$ and $\tilde{H}_{M_2M_1}^{(\prime)}$. Graphs with penguin topologies, discussed in section III C, produce the $P_{M_2,n}^p$ and $\tilde{P}_{M_2,n}^p$ functions, where n refers to the twist of the LCDA that enters the evaluation of the function. All of these functions consist of convolutions of hard-scattering kernels with meson light-cone distribution amplitudes, as will be shown below.

The scale at which renormalization scale dependent quantities are to be evaluated differs depending on the source of the contribution. In particular, while the vertex and penguin diagrams are evaluated at a scale $\mu \sim m_b$, the spectator scattering contributions are evaluated at a lower scale $\mu_h \sim \sqrt{m_b \Lambda_{\text{QCD}}}$. This applies to all scale dependent quantities multiplying the spectator scattering functions $H^{(\prime)}$, including the Wilson coefficients [24].

A. Vertex Diagrams

The first class of diagrams we consider are those shown in Figure 2 in which a hard gluon is exchanged between the emission meson M_2 and the quarks involved in the $B \rightarrow M_1$ transition. These amplitudes are proportional to both f_{M_2} and $F_0^{B \rightarrow M_1}(0)$ and contribute to the kernel T^I in (4). In terms of the coefficients a_i in (15) they produce $V_{M_2}^{(\prime)}$ at $\mathcal{O}(\alpha_s)$ and $\tilde{V}_{M_2}^{(\prime)}$ at $\mathcal{O}(\alpha_s^2 \beta_0)$.

Although when evaluated in $D = 4 - 2\epsilon$ dimensions each of these diagrams contains a $1/\epsilon^2$ pole from infrared and collinear divergences, these cancel in the sum of the four diagrams, leaving a residual UV $1/\epsilon$ pole to be renormalized. We renormalize in the $\overline{\text{MS}}$ scheme, treating γ_5 in the naive dimensional regularization (NDR) prescription [51]. For

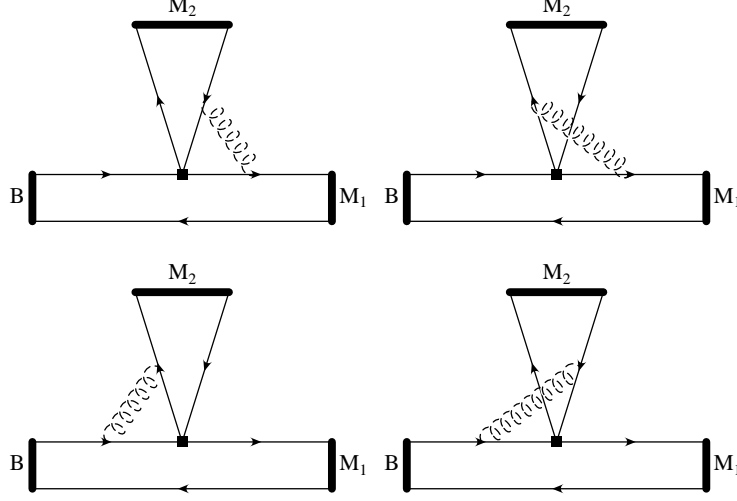


FIG. 2: The factorization-breaking vertex diagrams.

completeness we restate the result of Ref. [24] for the $\mathcal{O}(\alpha_s)$ contributions

$$V_M = -6 \left[\ln \left(\frac{\mu^2}{m_b^2} \right) + \frac{5}{3} \right] - 1 + \int_0^1 dx g(x) \Phi_M(x) \quad (16)$$

and

$$V'_M = -6 \left[\ln \left(\frac{\mu^2}{m_b^2} \right) + \frac{5}{3} \right] + 11 + \int_0^1 dx g(1-x) \Phi_M(x) \quad (17)$$

where the integration kernel is

$$g(x) = \left[\frac{3(1-2x)}{2(1-x)} \ln(x) - \frac{1}{2} (7 + 3i\pi) + (x \leftrightarrow \bar{x}) \right] + \left[\frac{\ln(x)}{2(1-x)} - 2i\pi \ln(x) - \ln^2(x) - 2\text{Li}_2(1-x) - (x \leftrightarrow \bar{x}) \right]. \quad (18)$$

For the next order result we find

$$\tilde{V}_M = -3 \left[\ln \left(\frac{\mu^2}{m_b^2} \right) + \frac{5}{3} \right]^2 + \left[\ln \left(\frac{\mu^2}{m_b^2} \right) + \frac{5}{3} \right] \int_0^1 dx g(x) \Phi_M(x) + \int_0^1 dx h(x) \Phi_M(x) - \frac{65}{12} \quad (19)$$

and

$$\tilde{V}'_M = -3 \left[\ln \left(\frac{\mu^2}{m_b^2} \right) + \frac{5}{3} \right]^2 + \left[\ln \left(\frac{\mu^2}{m_b^2} \right) + \frac{5}{3} \right] \int_0^1 dx g(1-x) \Phi_M(x) + \int_0^1 dx h(1-x) \Phi_M(x) - \frac{5}{12}. \quad (20)$$

The function $h(x)$ appearing in this expression is given by

$$h(x) = \left[-\frac{3(1-3x)}{4(1-x)} \ln^2(x) + \left(\frac{7(1-2x)}{4(1-x)} + \frac{3}{2}i\pi \right) \ln(x) + \frac{3x\text{Li}_2(1-x)}{2(1-x)} \right]$$

$$\begin{aligned}
& \left. -\frac{1}{4} (15 + 7i\pi) + (x \leftrightarrow \bar{x}) \right] \\
& + \left[\ln^3(x) - \left(\frac{5-3x}{4(1-x)} + 2\ln(1-x) - i\pi \right) \ln^2(x) + \left(\frac{1}{4(1-x)} + 2\pi^2 - \frac{3}{2}i\pi \right) \ln(x) \right. \\
& \quad \left. - \frac{4-3x}{2(1-x)} \text{Li}_2(1-x) - 2\text{Li}_3(1-x) - 4\text{Li}_3(x) - (x \leftrightarrow \bar{x}) \right]. \quad (21)
\end{aligned}$$

This function has previously been derived in [42]; we confirm that result.

One may notice from a comparison of the factorized operator (13) with the pattern of vertex graph contributions to the a_i coefficients in (15) that the unprimed functions V, \tilde{V} are associated with $(V - A) \otimes (V - A)$ operator structures, while V', \tilde{V}' are associated with $(V - A) \otimes (V + A)$ structures. The remaining operator structure present in (13) is $(S - P) \otimes (S + P)$, and this receives a nonzero vertex contribution only when the twist-3 LCDAs Φ_p are included. We have used the fact that, in the approximation of including only the ‘chirally enhanced’ terms at twist-3, Φ_p has its asymptotic form $\Phi_p(x) = 1$ to carry out the momentum fraction integrals, resulting in the constants ‘-6’ and ‘-4’ appearing in a_6 of (15) at $\mathcal{O}(\alpha_s)$ and $\mathcal{O}(\alpha_s^2\beta_0)$, respectively.

Using the Gegenbauer expansion for the LCDAs Φ_M , we carry out the integration over momentum fraction x to obtain

$$\begin{aligned}
\int_0^1 dx g(x) \Phi_M(x) &= -\frac{15}{2} - 3i\pi + \left(\frac{11}{2} - 3i\pi \right) \alpha_1^M \\
&\quad - \frac{21}{20} \alpha_2^M + \left(\frac{79}{36} - \frac{2}{3}i\pi \right) \alpha_3^M + \dots \quad (22)
\end{aligned}$$

and

$$\begin{aligned}
\int_0^1 dx h(x) \Phi_M(x) &= \pi^2 - \frac{33}{2} - 6i\pi + \left(3\pi^2 + \frac{65}{6} - \frac{11}{2}i\pi \right) \alpha_1^M \\
&\quad + \left(\frac{3}{2}\pi^2 - \frac{7359}{400} - \frac{9}{10}i\pi \right) \alpha_2^M + \left(\frac{5}{18}\pi^2 + \frac{10481}{720} - \frac{37}{15}i\pi \right) \alpha_3^M + \dots \quad (23)
\end{aligned}$$

Thus the vertex diagrams introduce complex phases into the amplitude, and the magnitude of the phase depends on the shape of the LCDAs parametrized by α_i^M .

B. Spectator Scattering Diagrams

The two diagrams involving hard scattering with the spectator quark are shown in Figure 3. The $\mathcal{O}(\alpha_s)$ corrections are expressed in Ref. [24] in terms of two functions $H_{M_2 M_1}^{(\prime)}$ as shown in (15). We choose to write these functions as

$$\begin{aligned}
H_{M_2 M_1}^{(\prime)} &= \frac{f_B f_{M_1}}{m_B^2 F_0^{B \rightarrow M_1}(0)} \int_0^1 dx \int_0^1 dy \int_0^1 d\xi \left[{}_2 H_{M_2 M_1}^{(\prime)}(x, y, \xi) \Phi_{M_2}(x) \Phi_{M_1}(y) \Phi_B(\xi) \right. \\
&\quad \left. + \frac{2\mu_{M_1}}{m_b} {}_3 H_{M_2 M_1}^{(\prime)}(x, y, \xi) \Phi_{M_2}(x) \Phi_p^{M_1}(y) \Phi_B(\xi) \right]. \quad (24)
\end{aligned}$$

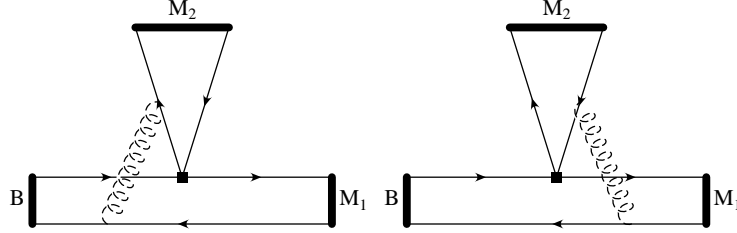


FIG. 3: The factorization-breaking spectator scattering diagrams.

where we have divided the integration kernel into twist-2 (${}_2H^{(\prime)}$) and twist-3 (${}_3H^{(\prime)}$) components. In the approximation $\xi \ll x, y$, which one expects to be valid through most of phase space, the integration kernels are

$$\begin{aligned} {}_2H_{M_2M_1}(x, y, \xi) &= {}_3H'_{M_2M_1}(x, y, \xi) = \frac{1}{\bar{x} \bar{y} \xi}, \\ {}_2H'_{M_2M_1}(x, y, \xi) &= {}_3H_{M_2M_1}(x, y, \xi) = \frac{1}{x \bar{y} \xi}. \end{aligned} \quad (25)$$

If one replaces the light-cone distribution functions Φ_M with their expansions in terms of Gegenbauer polynomials (10) and carries out the integrations in (24), one finds

$$\begin{aligned} H_{M_2M_1}^{(\prime)} &= \frac{f_B f_{M_1}}{m_B \lambda_B F_0^{B \rightarrow M_1}(0)} \left[9(1 + \alpha_1^{M_1} + \alpha_2^{M_1} + \dots)(1 \pm \alpha_1^{M_2} + \alpha_2^{M_2} \pm \dots) \right. \\ &\quad \left. + \frac{6\mu_{M_1}}{m_b} X_H^{M_1} (1 \mp \alpha_1^{M_2} + \alpha_2^{M_2} \mp \dots) \right] \end{aligned} \quad (26)$$

where the ellipses denote higher order Gegenbauer moments, and in ‘ \pm/\mp ’ the top symbol applies to H and the bottom symbol to H' . Following Refs. [22, 23, 24] we have also introduced two parameters λ_B and $X_H^{M_1}$ defined by

$$\int_0^1 d\xi \frac{\Phi_B(\xi)}{\xi} \equiv \frac{m_B}{\lambda_B}; \quad \int_0^1 dy \frac{\Phi_p^{M_1}(y)}{\bar{y}} \equiv X_H^{M_1}. \quad (27)$$

Because the light quark in the B meson carries a small momentum fraction, the wavefunction $\Phi_B(\xi)$ has support only for $0 < \xi \lesssim \Lambda_{\text{QCD}}/m_b$. The definition (27) then implies $\lambda_B \sim \Lambda_{\text{QCD}}$. It is necessary to introduce the parameter $X_H^{M_1}$ because, with the asymptotic form for $\Phi_p^{M_1} = 1$, the integration contains a logarithmic divergence when the B meson spectator quark enters M_1 as a soft quark $\bar{y} \sim 0$. This divergence is a consequence of our having neglected the small transverse components of momentum and quark off-shellness [24]. $X_H^{M_1}$ is therefore a new complex nonperturbative parameter, and by power counting it is of size $X_H^{M_1} \sim \ln(m_b/\Lambda_{\text{QCD}})$.

At next perturbative order one finds two new functions $\tilde{H}_{M_2M_1}^{(\prime)}$ defined by

$$\tilde{H}_{M_2M_1}^{(\prime)} = \left[\ln \left(\frac{\mu^2}{m_B^2} \right) + \frac{5}{3} \right] H_{M_2M_1}^{(\prime)}$$

$$\begin{aligned}
& - \frac{f_B f_{M_1}}{m_B^2 F_0^{B \rightarrow M_1}(0)} \int_0^1 dx \int_0^1 dy \int_0^1 d\xi \left[{}_2\tilde{H}_{M_2 M_1}^{(\prime)}(x, y, \xi) \Phi_{M_2}(x) \Phi_{M_1}(y) \Phi_B(\xi) \right. \\
& \left. + \frac{2\mu_{M_1}}{m_b} {}_3\tilde{H}_{M_2 M_1}^{(\prime)}(x, y, \xi) \Phi_{M_2}(x) \Phi_p^{M_1}(y) \Phi_B(\xi) \right] \quad (28)
\end{aligned}$$

where the new hard scattering kernels are

$$\begin{aligned}
{}_2\tilde{H}_{M_2 M_1}(x, y, \xi) &= {}_3\tilde{H}'_{M_2 M_1}(x, y, \xi) = \frac{\ln(\xi \bar{y})}{\bar{x} \bar{y} \xi}, \\
{}_2\tilde{H}'_{M_2 M_1}(x, y, \xi) &= {}_3\tilde{H}_{M_2 M_1}(x, y, \xi) = \frac{\ln(\xi \bar{y})}{x \bar{y} \xi}. \quad (29)
\end{aligned}$$

Carrying out the integrations explicitly one arrives at

$$\begin{aligned}
\tilde{H}_{M_2 M_1}^{(\prime)} &= \left[\ln \left(\frac{\mu^2}{m_B^2} \right) + \frac{5}{3} \right] H_{M_2 M_1}^{(\prime)} \\
&+ \frac{f_B f_{M_1}}{m_B F_0^{B \rightarrow M_1}(0)} \left[\frac{27}{2\lambda_B} \left(1 + \frac{17}{9} \alpha_1^{M_1} + \frac{43}{18} \alpha_2^{M_1} + \dots \right) \left(1 \pm \alpha_1^{M_2} + \alpha_2^{M_2} \pm \dots \right) \right. \\
&- \frac{9}{\tilde{\lambda}_B} \left(1 + \alpha_1^{M_1} + \alpha_2^{M_1} + \dots \right) \left(1 \pm \alpha_1^{M_2} + \alpha_2^{M_2} \pm \dots \right) \\
&\left. - \frac{6\mu_{M_1}}{m_b} \left\{ \frac{\tilde{X}_H^{M_1}}{\lambda_B} + \frac{X_H^{M_1}}{\tilde{\lambda}_B} \right\} \left(1 \mp \alpha_1^{M_2} + \alpha_2^{M_2} \mp \dots \right) \right]. \quad (30)
\end{aligned}$$

The large coefficients in the second line of (30) result from the integral $\int_0^1 \ln \bar{y} \Phi(y) / \bar{y} dy$. In the Gegenbauer expansion of the LCDA Φ all of the Gegenbauer moments α_i enter with large coefficients, so only if the moments themselves decrease quickly will this integral be well represented by the terms we retain. In addition we have been forced to introduce two additional parameters similar to those in (27):

$$\int_0^1 d\xi \frac{\ln \xi \Phi_B(\xi)}{\xi} \equiv \frac{m_B}{\tilde{\lambda}_B}; \quad \int_0^1 dy \frac{\ln \bar{y} \Phi_p^{M_1}(y)}{\bar{y}} \equiv \tilde{X}_H^{M_1}. \quad (31)$$

By power counting these parameters are of order $\tilde{\lambda}_B \sim \Lambda_{\text{QCD}} / \ln(\Lambda_{\text{QCD}}/m_b)$ and $\tilde{X}_H^{M_1} \sim \text{Li}_2(-m_b/\Lambda_{\text{QCD}})$.

C. QCD Penguin Diagrams

An important source of strong phases in the decay amplitudes are the QCD penguin diagrams, shown in Figure 4. These diagrams give rise to the functions $P_{M,i}^p$ and $\tilde{P}_{M,i}^p$ appearing in (15). The four quark operators in the Hamiltonian (3) contribute to the left-hand diagram, while the chromomagnetic dipole operator \mathcal{O}_{8g} contributes in the right-hand diagram.

We begin by stating the results at $\mathcal{O}(\alpha_s)$. At twist-2 one finds [24]

$$\begin{aligned}
P_{M,2}^p &= \int_0^1 dx P_2^p(x) \Phi_M(x) \\
P_2^p(x) &= C_1 \left[\frac{4}{3} \ln \frac{m_b}{\mu} + \frac{2}{3} - G(s_p, x) \right] + C_3 \left[\frac{8}{3} \ln \frac{m_b}{\mu} + \frac{4}{3} - G(0, x) - G(1, x) \right] \\
&\quad + (C_4 + C_6) \left[\frac{4n_f}{3} \ln \frac{m_b}{\mu} - (n_f - 2)G(0, x) - G(s_c, x) - G(1, x) \right] \\
&\quad - 2C_{8g}^{\text{eff}} \frac{1}{1-x}
\end{aligned} \tag{32}$$

where $n_f = 5$ is the number of active quark flavours, $s_q = (m_q/m_b)^2$, and $C_{8g}^{\text{eff}} = C_{8g} + C_5$.

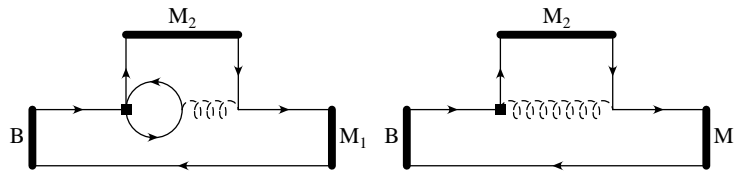


FIG. 4: The penguin and magnetic dipole diagrams.

The function $G(s, x)$ in (32) is given by the integral

$$G(s, x) = -4 \int_0^1 du u(1-u) \ln[s - u(1-u)(1-x) - i\epsilon]. \tag{33}$$

The integral $\int_0^1 dx G(s_p, x) \Phi(x)$ is complex and contributes to the strong phase of the amplitude for $s < 1/4$; that is, for all quark flavours except the b quark.

The order $\mathcal{O}(\alpha_s^2 \beta_0)$ results at twist-2 we find to be

$$\tilde{P}_{M,2}^p = \left[\ln \left(\frac{\mu^2}{m_b^2} \right) + \frac{5}{3} \right] P_{M,2}^p - \int_0^1 dx \ln(x-1-i\epsilon) P_2^p(x) \Phi_M(x). \tag{34}$$

A similar situation exists when one turns to the twist-3 terms. One finds the leading corrections involve

$$\begin{aligned}
P_{M,3}^p &= \int_0^1 dx P_3^p(x) \Phi_p^M(x) \\
P_3^p(x) &= C_1 \left[\frac{4}{3} \ln \frac{m_b}{\mu} + \frac{2}{3} - G(s_p, x) \right] + C_3 \left[\frac{8}{3} \ln \frac{m_b}{\mu} + \frac{4}{3} - G(0, x) - G(1, x) \right] \\
&\quad + (C_4 + C_6) \left[\frac{4n_f}{3} \ln \frac{m_b}{\mu} - (n_f - 2)G(0, x) - G(s_c, x) - G(1, x) \right] - 2C_{8g}^{\text{eff}}
\end{aligned} \tag{35}$$

where the twist-3 distribution function $\Phi_p^M(x)$ has replaced the twist-2 distribution in (32).

The $\mathcal{O}(\alpha_s^2 \beta_0)$ function is, in a manner closely analogous to (34), given by

$$\tilde{P}_{M,3}^p = \left[\ln \left(\frac{\mu^2}{m_b^2} \right) + \frac{5}{3} \right] P_{M,3}^p - \int_0^1 dx \ln(x-1-i\epsilon) P_3^p(x) \Phi_p^M(x). \tag{36}$$

The expressions which result from carrying out the integrations over momentum fractions are quite complicated for the penguin diagrams, and we refrain from presenting them here.

IV. PHENOMENOLOGICAL ANALYSIS

In this section we take the analytic results of section III and study direct CP asymmetries for various $\pi\pi$ and πK final states. We begin by giving the expressions for the decay amplitudes and the definitions for the CP asymmetries. In the next subsection we collect and discuss the input parameters we use to obtain numerical results. This is followed by a presentation and discussion of the results.

A. Definitions of Branching Ratios and CP Asymmetries

In terms of the coefficients a_i and the factorized matrix elements defined by

$$A_{M_1 M_2} = i \frac{G_F}{\sqrt{2}} (m_B^2 - m_{M_1}^2) F_0^{B \rightarrow M_1}(m_{M_2}^2) f_{M_2}, \quad (37)$$

the $B \rightarrow \pi K$ decay amplitudes are

$$\begin{aligned} \mathcal{A}(B^- \rightarrow \pi^- \bar{K}^0) &= \lambda_p \left[a_4^p + \frac{2\mu_K}{m_b} a_6^p \right] A_{\pi K}, \\ -\sqrt{2} \mathcal{A}(B^- \rightarrow \pi^0 K^-) &= \left[\lambda_u a_1 + \lambda_p a_4^p + \lambda_p \frac{2\mu_K}{m_b} a_6^p \right] A_{\pi K} + [\lambda_u a_2] A_{K\pi}, \\ -\mathcal{A}(\bar{B}^0 \rightarrow \pi^+ K^-) &= \left[\lambda_u a_1 + \lambda_p a_4^p + \lambda_p \frac{2\mu_K}{m_b} a_6^p \right] A_{\pi K}, \\ \sqrt{2} \mathcal{A}(\bar{B}^0 \rightarrow \pi^0 \bar{K}^0) &= \mathcal{A}(B^- \rightarrow \pi^- \bar{K}^0) + \sqrt{2} \mathcal{A}(B^- \rightarrow \pi^0 K^-) \\ &\quad - \mathcal{A}(\bar{B}^0 \rightarrow \pi^+ K^-). \end{aligned} \quad (38)$$

In these expressions $a_i \equiv a_i(\pi K)$, $\lambda_p = V_{ps}^* V_{pb}$, and a summation over $p \in \{u, c\}$ is implicit in expressions like $\lambda_p a_i^p$. The last relation is a consequence of isospin symmetry.

The $B \rightarrow \pi\pi$ decay amplitudes are given by

$$\begin{aligned} -\mathcal{A}(\bar{B}^0 \rightarrow \pi^+ \pi^-) &= \left[\lambda'_u a_1 + \lambda'_p a_4^p + \lambda'_p \frac{2\mu_\pi}{m_b} a_6^p \right] A_{\pi\pi}, \\ -\sqrt{2} \mathcal{A}(B^- \rightarrow \pi^- \pi^0) &= [\lambda'_u (a_1 + a_2)] A_{\pi\pi}, \\ \mathcal{A}(\bar{B}^0 \rightarrow \pi^0 \pi^0) &= \sqrt{2} \mathcal{A}(B^- \rightarrow \pi^- \pi^0) - \mathcal{A}(\bar{B}^0 \rightarrow \pi^+ \pi^-), \end{aligned} \quad (39)$$

where now $a_i \equiv a_i(\pi\pi)$ and $\lambda'_p = V_{ps}^* V_{pd}^*$. The CP conjugate decay amplitudes are obtained from the above by replacing $\lambda_p^{(l)} \rightarrow (\lambda_p^{(l)})^*$. Note that none of these decay modes are dependent on a_3 or a_5 . These factors, therefore, play no further role in our discussion.

CP violation can occur either directly via a difference between CP conjugate decay rates ($\Gamma(B \rightarrow f) \neq \Gamma(\bar{B} \rightarrow \bar{f})$) or, for neutral B mesons, indirectly via $B^0 - \bar{B}^0$ mixing. Accordingly, we treat the two cases separately.

For the decays $B^- \rightarrow \pi^- \bar{K}^0$, $B^- \rightarrow \pi^0 K^-$, and $\bar{B}^0 \rightarrow \pi^+ K^-$, the CP asymmetry is time independent and is defined as

$$\mathcal{A}_{\text{CP}}(\bar{f}) = \frac{|\mathcal{A}(\bar{B} \rightarrow \bar{f})|^2 - |\mathcal{A}(B \rightarrow f)|^2}{|\mathcal{A}(\bar{B} \rightarrow \bar{f})|^2 + |\mathcal{A}(B \rightarrow f)|^2} \quad (40)$$

where our sign convention is set by defining $\bar{B} = \bar{B}^0, B^-$ as an initial state containing a b quark, and $B = B^0, B^+$ as containing an initial b antiquark. This CP asymmetry vanishes in the limit of naive factorization, and first occurs at order α_s in the BBNS formalism. As such, it can be calculated to order $\alpha_s^2\beta_0$ with knowledge of only the next-to-leading order Wilson coefficients.

For the neutral B meson decays to final states f for which there are interference effects between $B^0 \rightarrow f$ and $B^0 \rightarrow \bar{B}^0 \rightarrow f$, the resulting CP asymmetry is time dependent

$$\mathcal{A}_{\text{CP}}(t, \bar{f}) = \frac{|\mathcal{A}(\bar{B}^0(t) \rightarrow \bar{f})|^2 - |\mathcal{A}(B^0(t) \rightarrow f)|^2}{|\mathcal{A}(\bar{B}^0(t) \rightarrow f)|^2 + |\mathcal{A}(B^0(t) \rightarrow f)|^2}. \quad (41)$$

In this paper the modes which fall into this class are $\bar{B}^0 \rightarrow \pi^0 K_S, \bar{B}^0 \rightarrow \pi^+\pi^-,$ and $\bar{B}^0 \rightarrow \pi^0\pi^0$. This asymmetry is often written as

$$\mathcal{A}_{\text{CP}}(t, \bar{f}) = \mathcal{A}_{\bar{f}} \cos(\Delta mt) - \mathcal{S}_{\bar{f}} \sin(\Delta mt) \quad (42)$$

where $\mathcal{A}_{\bar{f}}$ characterizes the direct CP violation due to interference of different diagrams contributing to the decay, and $\mathcal{S}_{\bar{f}}$ measures the indirect CP violation which originates from mixing between the B^0 and \bar{B}^0 initial states. Measuring the time dependence of the CP asymmetry allows one to separate the contributions of these two mechanisms.

Similar to the case of the time independent CP asymmetry above, $\mathcal{A}_{\bar{f}}$ first occurs at order α_s , and can be calculated with knowledge of only the leading order Wilson coefficients. Note that $\mathcal{A}_{\bar{f}}$ is simply the time dependent asymmetry evaluated at $t = 0$, and is given by (40). $\mathcal{S}_{\bar{f}}$ on the other hand is non-zero in naive factorization, and its determination requires knowledge of the NNLO Wilson coefficients. As such, we will not consider $\mathcal{S}_{\bar{f}}$ any further in this paper.

If we write the Feynman amplitudes (38)-(39) in the form $\mathcal{A} = \lambda_u^{(\prime)}u + \lambda_c^{(\prime)}c$ and decompose the two terms into perturbative contributions

$$\begin{aligned} u &= u_0 + \frac{\alpha_s}{4\pi}u_1 + \frac{\alpha_s^2}{(4\pi)^2}\beta_0u_2 \\ c &= c_0 + \frac{\alpha_s}{4\pi}c_1 + \frac{\alpha_s^2}{(4\pi)^2}\beta_0c_2 \end{aligned} \quad (43)$$

then we have

$$\mathcal{A}_{\text{CP}}^{\text{Dir}} = -2\text{Im}[\lambda_u^{(\prime)}(\lambda_c^{(\prime)})^*] \frac{\text{Im}[u^*c]}{|\lambda_u^{(\prime)}|^2|u|^2 + |\lambda_c^{(\prime)}|^2|c|^2 + 2\text{Re}[\lambda_u^{(\prime)}(\lambda_c^{(\prime)})^*]\text{Re}[u^*c]}. \quad (44)$$

We can expand $\mathcal{A}_{\text{CP}}^{\text{Dir}}$ to order $\mathcal{O}(\alpha_s^2\beta_0)$ to obtain

$$\begin{aligned} \mathcal{A}_{\text{CP}}^{\text{Dir}} &= \frac{2\text{Im}[\lambda_u^{(\prime)}(\lambda_c^{(\prime)})^*]}{(\lambda_u^{(\prime)}u_0 + \lambda_c^{(\prime)}c_0)((\lambda_u^{(\prime)})^*u_0 + (\lambda_c^{(\prime)})^*c_0)} \\ &\times \left\{ \frac{\alpha_s}{4\pi} (u_0\text{Im}[c_1] - c_0\text{Im}[u_1]) + \frac{\alpha_s^2}{(4\pi)^2}\beta_0 (u_0\text{Im}[c_2] - c_0\text{Im}[u_2]) \right\} \end{aligned} \quad (45)$$

where we have used the fact that u_0 and c_0 are real. Note that to this order the direct CP asymmetry is not sensitive to the real part of the perturbative corrections. Note also that, as anticipated, we require only the next-to-leading order behaviour of the Wilson coefficients.

B. Comparison to Previous Work

As mentioned earlier, the calculations presented in this paper are similar to calculations presented earlier by Neubert and Pecjak in [40]. Performing a renormalon analysis, they estimated both perturbative and power corrections in the context of the large- β_0 limit. This limit is a way of organizing the perturbative expansion that differs from what is typically done in renormalization group improved (RG-improved) perturbation theory. The most important difference is the power counting. Rather than expanding in the strong coupling, β_0 is taken to be large and one expands in powers of $1/\beta_0$. α_s is still considered to be a small parameter in this limit and scales like $\alpha_s \sim \mathcal{O}(1/\beta_0)$. In practice the large- β_0 scaling is implemented by switching to a rescaled coupling $b(\mu)$ related to the leading order running of α_s :

$$\alpha_s(\mu) \rightarrow b(\mu) = \beta_0 \frac{\alpha_s(\mu)}{4\pi} = \frac{1}{\log(\mu^2/\Lambda_{\overline{\text{MS}}}^2)}, \quad (46)$$

where $b(\mu) \sim \mathcal{O}(1)$. In contrast to RG-improved perturbation theory, $\log(M/\mu)$ is of $\mathcal{O}(1)$ in the large- β_0 limit. Furthermore, before one expands in $1/\beta_0$, all occurrences of n_f are replaced by $n_f \rightarrow -3\beta_0/2$.

This unusual counting scheme forces one to sum certain classes of diagrams to all orders in perturbation theory. The fermion bubbles of Fig. 1 are a special case as they scale as $\alpha_s\beta_0 \sim \mathcal{O}(1)$ after the replacement $n_f \rightarrow -3\beta_0/2$. Thus one must sum an infinite number of fermion bubbles into gluon propagators. The use of such summations is a common technique in renormalon analyses [52].

In [40], in order to calculate the a_i to subleading order, both the hard scattering kernels and the Wilson coefficients had to be calculated to NLO in the large- β_0 limit. As the hard scattering kernels are $\mathcal{O}(1)$, the Wilson coefficients had to be calculated to $\mathcal{O}(1/\beta_0)$. Because they are determined by matching at the weak scale ($\mu = m_W$) and running down to the scale of the decay ($\mu \sim m_b$), it was necessary to have the $\mathcal{O}(1/\beta_0)$ matching as well. However, it was argued by the authors that the difference between the NLO matching and $\mathcal{O}(1/\beta_0)$ matching was negligible so that the currently known one-loop (NLO) matching was sufficient.

To run the Wilson coefficients correctly, the elements of the anomalous dimension matrix had to be determined to the appropriate order. Because the current-current operators enter at $\mathcal{O}(1)$ in the matching, pieces of the anomalous dimension matrix which depend on these operators were determined to $\mathcal{O}(1/\beta_0)$. Current-current operators affect the running of both the penguin operators and the current-current operators themselves. For the penguin operators, their effect can be determined from the LO anomalous dimension matrix in [43]. For

the current-current operators this has been calculated in [53]. Penguin operators enter at order $\mathcal{O}(1/\beta_0)$ at the matching scale. As such, to calculate the elements of the anomalous dimension matrix which depend on the penguin operators, it was only necessary to calculate the diagrams to $\mathcal{O}(1)$. Unlike the current-current operators, penguin diagrams in the effective theory can be of $\mathcal{O}(1)$ because of factors of n_f which occur in fermion loops.

In contrast, the calculations we perform in this paper are in the context of the usual RG-improved perturbation theory, where $\log(M/\mu) \sim \mathcal{O}(1/\alpha_s)$, and one calculates order by order in α_s . We have calculated the hard scattering kernels to $\mathcal{O}(\alpha_s^2\beta_0)$. This corresponds to inserting a single fermion bubble into the gluon propagators of the $\mathcal{O}(\alpha_s)$ diagrams and replacing $n_f \rightarrow -3\beta_0/2$. Both the previous authors and ourselves had to decide what to do about the factors of n_f which appear in the penguin diagrams. The factors of n_f which enter from the fermion bubble have corresponding diagrams with gluon and ghost loops which justify their replacement, but these diagrams are not present for other factors of n_f which emerge from penguin diagrams. The previous authors took two different approaches to this problem and considered the cases where they either replaced $n_f \rightarrow -3\beta_0/2$ or they left these factors of n_f alone. They achieved better results from the second approach, which is physically better justified. We choose to use only this latter approach in this paper.

To further aid in our calculations, we choose to calculate quantities that first occur at $\mathcal{O}(\alpha_s)$ in perturbation theory. It is easily understood that such quantities require only the NLO Wilson coefficients from [43]. The leading order terms in the Wilson coefficients sum logs of the form $\alpha_s^n \log^n(M/\mu)$ and scale as $\mathcal{O}(1)$. The NLO terms sum logs of the form $\alpha_s^{n+1} \log^n(M/\mu)$ and scale as $\mathcal{O}(\alpha_s)$. Because a two loop calculation is necessary to calculate these NLO terms they may contain factors of β_0 in the form

$$\alpha_s^{n+2}\beta_0 \log^{n+1}(M/\mu) \sim \alpha_s\beta_0. \quad (47)$$

If we were only after a $\mathcal{O}(\alpha_s)$ result, we would need the $\mathcal{O}(1)$ (LO) Wilson coefficient and the $\mathcal{O}(\alpha_s)$ hard scattering kernel. At $\mathcal{O}(\alpha_s^2\beta_0)$ however, we need not only the $\mathcal{O}(1)$ Wilson coefficient and the $\mathcal{O}(\alpha_s^2\beta_0)$ hard scattering kernel, but also the $\mathcal{O}(\alpha_s)$ (NLO) Wilson coefficient and the $\mathcal{O}(\alpha_s)$ hard scattering kernel. Since we only need the piece of the NLO Wilson coefficient proportional to β_0 we are effectively keeping some unnecessary higher order pieces. Either way, we require only the NLO Wilson coefficients.

An important effect of the differences between the two approaches is reflected in the different contributions to the hard scattering kernels which must be calculated. In order to calculate the coefficients (15), we need many hard scattering and vertex contributions. Neubert and Pecjak needed fewer of these contributions, but those they did need were needed to all orders in $\alpha_s^{n+1}\beta_0^n$. This difference has important phenomenological effects. The contributions we include are sensitive to unknown non-perturbative parameters. As we will see, these parameters can introduce a large uncertainty in various observables.

TABLE I: Numerical values of the Wilson coefficients C_i in the NDR scheme at NLO, in units of 10^{-3} . We have used the input parameters $\Lambda_{\text{QCD}} = 223 \text{ MeV}$, $m_t = 174 \text{ GeV}$, $m_b = 4.2 \text{ GeV}$, and $m_W = 80.4 \text{ GeV}$. The soft scales are defined using $\Lambda_h = 500 \text{ MeV}$.

	μ					
	$\sqrt{\Lambda_h m_b/2}$	$\sqrt{\Lambda_h m_b}$	$\sqrt{\Lambda_h 2m_b}$	$m_b/2$	m_b	$2m_b$
C_1	1258.0	1195.2	1150.4	1147.7	1087.8	1048.6
C_2	-474.8	-378.7	-305.3	-300.7	-193.3	-114.4
C_3	35.7	27.4	21.6	21.2	13.8	9.0
C_4	-77.7	-62.8	-52.0	-51.3	-36.0	-25.0
C_5	11.9	12.4	11.9	11.9	9.9	7.7
C_6	-118.6	-88.2	-68.5	-67.4	-43.3	-28.3
C_{8g}^{eff}	-	-	-	-169.0	-151.0	-136.0

C. Input Data

The numerical analysis in section IV D requires various parameters as theoretical inputs. In this section we collect these input parameters together.

1. Model Independent Parameters

For the running coupling $\alpha_s(\mu)$ we use

$$\alpha_s(\mu) = \frac{4\pi}{\beta_0 \ln(\mu^2/\Lambda_{\text{QCD}}^2)} \left[1 - \frac{\beta_1}{\beta_0^2} \frac{\ln(\ln(\mu^2/\Lambda_{\text{QCD}}^2))}{\ln(\mu^2/\Lambda_{\text{QCD}}^2)} \right] \quad (48)$$

where, in terms of the number of colors N_c and flavours n_f ,

$$\beta_0 = \frac{11N_c - 2n_f}{3}, \quad \beta_1 = \frac{34N_c^2}{3} - \frac{10N_c n_f}{3} - 2C_F n_f, \quad C_F = \frac{N_c^2 - 1}{2N_c}. \quad (49)$$

We take $\Lambda_{\text{QCD}} = 223 \text{ MeV}$, which is equivalent to running with $n_f = 5$ flavours from $\alpha_s(M_Z) = 0.1185$.

The Wilson coefficients calculated to NLO in QCD are shown in Table I.

We choose to work in the Wolfenstein parametrization

$$V_{\text{CKM}} = \begin{pmatrix} 1 - \frac{\lambda^2}{2} & \lambda & A\lambda^3(\rho - i\eta) \\ -\lambda & 1 - \frac{\lambda^2}{2} & A\lambda^2 \\ A\lambda^3(1 - \rho - i\eta) & -A\lambda^2 & 1 \end{pmatrix} + \mathcal{O}(\lambda^4). \quad (50)$$

In the analysis below we will sometimes plot observables as a function of the unitarity angle $\gamma = \text{Arg}[V_{ub}^*]$. In that case we write $(\rho - i\eta) = \sqrt{\rho^2 + \eta^2} e^{-i\gamma}$. We take the numerical values

of the CKM parameters from a recent global fit [54]: $A = 0.83 \pm 0.04$, $\lambda = 0.2224 \pm 0.0020$, $\sqrt{\rho^2 + \eta^2} = 0.398 \pm 0.040$, and $\gamma = (64 \pm 11)^\circ$.

For the B meson lifetimes we use the PDG values [55]: $\tau(\bar{B}^0) = 1.536 \pm 0.014 ps$ and $\tau(B^\pm) = 1.671 \pm 0.018 ps$. Our quark pole masses are $m_b = 4.2 GeV$, $m_c = 1.3 GeV$, and we set $m_{s,u,d} = 0$. Finally, for the ‘chiral enhancement’ factor defined in (7), which is a renormalization scale dependent quantity, we use [36]

$$\mu_P(m_b/2) = 0.85 \frac{m_b}{2}, \quad \mu_P(m_b) = 1.14 \frac{m_b}{2}, \quad \mu_P(2m_b) = 1.42 \frac{m_b}{2} \quad (51)$$

for both $P = \pi, K$.

2. Model Dependent Parameters

The matrix element for a B transition to a pseudoscalar state M is given by

$$\langle M(q) | \bar{q} \gamma^\mu b | \bar{B}(h) \rangle = F_+^{B \rightarrow M}(p^2)(h^\mu + q^\mu) + [F_0^{B \rightarrow M}(p^2) - F_+^{B \rightarrow M}(p^2)] \frac{m_B^2 - m_M^2}{p^2} p^\mu \quad (52)$$

where the momentum transfer is $p = h - q$. In practice this matrix element is always contracted with one of the meson momenta, and using the Dirac equation it is always possible to write these contractions in terms of $\langle M(q) | \bar{q} \not{p} b | \bar{B}(h) \rangle = F_0^{B \rightarrow M}(p^2)(m_B^2 - m_M^2)$, so that dependence on F_+ drops out. Since we are studying mesons with mass small compared to the B mass, we need consider only the point $F_0^{B \rightarrow M}(0)$. Estimates of this quantity have been made from QCD light-cone sum rules [56, 57, 58], relativistic quark models [59], and lattice calculations [60], with good agreement between the various methods. Numerically we take

$$F_0^{B \rightarrow K}(0) = \frac{f_K}{f_\pi} F_0^{B \rightarrow \pi}(0); \quad F_0^{B \rightarrow \pi}(0) = 0.258 \pm 0.031 GeV. \quad (53)$$

The decay constants f_M are defined by

$$\langle M(p) | \bar{q} \gamma^\mu \gamma_5 q | 0 \rangle = -i f_M p^\mu. \quad (54)$$

In our data analysis we will take

$$f_\pi = 0.1307 \pm 0.0004 GeV [55], \quad f_K = 0.1598 \pm 0.0016 GeV [55], \quad f_B = 0.180 \pm 0.040 GeV [61]. \quad (55)$$

The general decomposition of the LCDAs Φ_M has been given earlier (10) in terms of the parameters α_i^M , and throughout section III we stated our results in terms of these parameters. A variety of phenomenological and sum rule estimates have been made for these parameters [45, 49, 50, 62], and we adopt the values

$$\begin{aligned} \alpha_1^\pi &= 0, & \alpha_2^\pi &= 0.1 \pm 0.3, \\ \alpha_1^K &= 0.10 \pm 0.12, & \alpha_2^K &= 0.1 \pm 0.3. \end{aligned} \quad (56)$$

Owing to their nonperturbative origin all of these parameters are rather poorly known, and this is indicated by the conservative error estimates. The exception to this rule is α_1^π which deviates from zero only by $SU(2)$ breaking effects.

Little is known about the LCDA for the light quark in the B meson. Accordingly, in section III B we, following Ref. [24], parametrized the integrals over Φ_B that we encountered:

$$\int_0^1 d\xi \frac{\Phi_B(\xi)}{\xi} = \frac{m_B}{\lambda_B} \sim \frac{m_B}{\Lambda_h}, \quad \int_0^1 d\xi \frac{\ln \xi \Phi_B(\xi)}{\xi} = \frac{m_B}{\tilde{\lambda}_B} \sim \frac{m_B}{\Lambda_h} \ln \left(\frac{\Lambda_h}{m_B} \right) \quad (57)$$

where we take the soft scale to be $\Lambda_h = 500$ MeV. In our numerical analysis we assign a 100% uncertainty to these integrals, varying $0 < m_B/\lambda_B < 2(m_B/\Lambda_h)$ and $0 < -m_B/\tilde{\lambda}_B < 2(m_B/\Lambda_h \ln(m_B/\Lambda_h))$ with a uniform probability distribution.

Also in section III B we saw that integrals over the twist-3 LCDAs required the introduction of two other parameters

$$\int_0^1 dy \frac{\Phi_p^{M_1}(y)}{\bar{y}} = X_H^{M_1}, \quad \int_0^1 dy \frac{\ln \bar{y} \Phi_p^{M_1}(y)}{\bar{y}} = \tilde{X}_H^{M_1}. \quad (58)$$

The approximate magnitude of these parameters can be estimated by power counting, but in general they can be complex. Therefore, following Ref. [24] we write them as

$$X_H^{M_1} = \left(1 + \rho_H e^{i\phi_H}\right) \ln \left(\frac{m_B}{\Lambda_h}\right), \quad \tilde{X}_H^{M_1} = \left(1 + \tilde{\rho}_H e^{i\tilde{\phi}_H}\right) \text{Li}_2 \left(\frac{-m_b}{\Lambda_h}\right). \quad (59)$$

In the numerical analysis below we vary $0 < \rho_H, \tilde{\rho}_H < 2$ and allow the phases $\phi_H, \tilde{\phi}_H$ to take arbitrary values.

In the numerical analysis which follows, our central values are obtained by setting all of the input parameters at the center of their ranges. For the arbitrary phases in X_H and \tilde{X}_H we must choose a particular value for our 'central value'. We choose $\phi_H, \tilde{\phi}_H = \pi/2$, which makes the real and imaginary parts of the central values of X_H and \tilde{X}_H of equal magnitude.

D. Results

The main numerical results of this paper are presented in Table II which shows the results for the direct CP asymmetries $\mathcal{A}_{\text{CP}}^{\text{Dir}}$. After a general discussion of the results, we include a more detailed discussion of the particular asymmetry $\mathcal{A}_{\text{CP}}^{\text{Dir}}(\pi^+\pi^-)$. For each quantity we first state the prediction at $\mathcal{O}(\alpha_s)$, then the $\mathcal{O}(\alpha_s^2\beta_0)$ correction and, finally, the sum. We also state the results at three different renormalization scales.

In addition, we estimate the uncertainties arising from the model dependent parameters discussed in section IV C 2. We divide these parameters into three groups. The Gegenbauer moments $\alpha_{1,2}$ which parametrize the shape of the LCDAs, are varied with the 1σ error bars given in (56). The B decay formfactor $F_0^{B \rightarrow \pi}(0)$ and B meson decay constant f_B are varied with the 1σ error bars given in (53) and (55), respectively. Finally, the parameters arising

from the spectator scattering graph $(\lambda_B, \tilde{\lambda}_B, X_H, \tilde{X}_H)$ are varied with equal probability over the ranges given in section IV C 2 above. These three groups are labelled LCDA $(\alpha_{1,2}^{\pi,K})$, FF $(f_B, F_0^{B \rightarrow \pi}(0))$, and SPEC $(\lambda_B, \tilde{\lambda}_B, X_H, \tilde{X}_H)$ in our Table. The sets of parameters are varied independently, and in all cases the uncertainties we give are 1σ standard deviations. Note that there are additional sources of uncertainty we do not consider, such as dependence on the CKM matrix elements and quark masses. Our analysis does, however, give insight into the relative size of perturbative corrections and nonperturbative uncertainties.

1. CP asymmetries

Table II contains our results for the direct CP asymmetries $\mathcal{A}_{\text{CP}}^{\text{Dir}}$. It should be noted that the values in Table II do not take into account the contribution from weak annihilation diagrams and as such should not be taken as rigorous predictions of the BBNS method. They are however valid for their purpose of studying the perturbative behaviour of the formalism. Notice that the asymmetry $\mathcal{A}_{\text{CP}}(\pi^-\pi^0)$ is not shown in the table; as is clear from the definitions (39), the amplitude for $B^- \rightarrow \pi^-\pi^0$ has only one weak phase and therefore the asymmetry for this mode is zero (up to small electroweak corrections which we have neglected). The final column of Table II gives the current experimental values for the CP asymmetries. They are from HFAG, Summer 2005 compilation [63], apart from the observables where different experiments do not agree, in which case the errors are inflated according to the PDG prescription [55].

Though the relative sizes of the perturbative contributions at $\mathcal{O}(\alpha_s)$ and $\mathcal{O}(\alpha_s^2\beta_0)$ in Table II are quite sensitive to the renormalization scale, it is generally true that the two contributions are of roughly the same size. This may be understood as follows: the asymmetries are dominated by the contributions from the penguin diagrams, and $\alpha_s\beta_0|\tilde{P}/P|/4\pi \sim 1$, where P and \tilde{P} refer to the penguin functions defined in section III C.

There is no reduction in the renormalization scale dependence of the asymmetries after adding the $\mathcal{O}(\alpha_s^2\beta_0)$ terms. This behaviour follows from our previous remarks: at a given scale, the $\mathcal{O}(\alpha_s^2\beta_0)$ contributions are numerically similar to the $\mathcal{O}(\alpha_s)$ contributions. The sum, therefore, follows the pattern established at $\mathcal{O}(\alpha_s)$.

The next to last columns of Table II show the sensitivity of the asymmetries to the three classes of parameters defined above. The dominant uncertainty for most of the modes is due to the light cone distribution amplitudes (LCDA). These parameters are similar in size for each decay mode (see (56)), and the asymmetry is proportional to them. Consequently the size of the uncertainty in this column scales roughly with the size of the asymmetry itself.

Note also that three of the modes – $\pi^0 K^-$, $\pi^0 K_S$, and $\pi^0\pi^0$ – are particularly sensitive to the form factor (FF) and spectator scattering (SPEC) parameters. Unlike other decay modes, the FF and SPEC parameters in these modes are proportional to the Wilson coefficient C_1 . The strong sensitivity in these modes is simply a reflection of the large size of C_1

TABLE II: Numerical results for direct CP asymmetries $\mathcal{A}_{\text{CP}}^{\text{Dir}}$, expressed in percent. We present the $\mathcal{O}(\alpha_s)$ and subleading $\mathcal{O}(\alpha_s^2\beta_0)$ perturbative corrections. Partial error estimates whose meaning is explained in the text and experimental values are also presented.

Decay Mode	μ	$\mathcal{O}(\alpha_s)$	$\mathcal{O}(\alpha_s^2\beta_0)$	Total	Error Estimates			Experiment
					LCDA	FF	SPEC	
$\mathcal{A}_{CP}(\pi^-\bar{K}^0)$	$m_b/2$	0.9	0.1	0.9	± 0.1	± 0.0	± 0.0	$-2. \pm 5.$
	m_b	1.0	0.3	1.2	± 0.1	± 0.0	± 0.0	
	$2m_b$	1.2	0.4	1.6	± 0.1	± 0.0	± 0.0	
$\mathcal{A}_{CP}(\pi^0 K^-)$	$m_b/2$	9.1	-1.4	7.7	± 2.5	± 0.5	± 1.4	$4. \pm 4.$
	m_b	15.9	8.3	24.2	± 3.0	$^{+0.6}_{-0.7}$	± 1.8	
	$2m_b$	29.4	28.9	58.2	± 4.1	$^{+0.8}_{-0.9}$	± 2.5	
$\mathcal{A}_{CP}(\pi^+ K^-)$	$m_b/2$	3.9	-3.1	0.7	± 2.2	± 0.0	± 0.1	-11.5 ± 1.8
	m_b	9.3	4.8	14.0	± 2.3	± 0.0	± 0.0	
	$2m_b$	19.2	20.1	39.3	± 3.1	± 0.0	± 0.1	
$\mathcal{A}_{CP}(\pi^0 K_S)$	$m_b/2$	-3.0	-1.2	-4.2	± 0.9	± 0.4	± 1.1	$2. \pm 13.$
	m_b	-3.2	-2.0	-5.2	± 1.0	± 0.4	± 1.2	
	$2m_b$	-4.5	-4.3	-8.8	± 1.1	$^{+0.5}_{-0.4}$	± 1.4	
$\mathcal{A}_{CP}(\pi^+ \pi^-)$	$m_b/2$	-2.6	1.6	-1.0	± 1.1	± 0.0	± 0.1	$37. \pm 23.$
	m_b	-3.6	-1.9	-5.6	± 0.7	± 0.0	± 0.0	
	$2m_b$	-4.2	-4.3	-8.5	± 0.5	± 0.0	± 0.0	
$\mathcal{A}_{CP}(\pi^0 \pi^0)$	$m_b/2$	68.6	28.8	97.4	± 16.0	$^{+10.7}_{-12.3}$	± 33.5	$28. \pm 40.$
	m_b	40.7	26.5	67.2	± 10.4	$^{+6.1}_{-6.9}$	± 19.2	
	$2m_b$	25.3	25.4	50.7	± 5.7	$^{+3.0}_{-3.4}$	± 9.5	

in comparison to the other Wilson coefficients.

On the other hand, the asymmetry $\mathcal{A}_{\text{CP}}^{\text{Dir}}(\pi^-\bar{K}^0)$ has no dependence on the form factors or spectator scattering parameters. This may be understood by examining our master formula for the CP asymmetry, Eq. (45),

$$\mathcal{A}_{\text{CP}}^{\text{Dir}} \propto \text{Im}[u^* c] = \frac{\alpha_s}{4\pi} (u_0 \text{Im}[c_1] - c_0 \text{Im}[u_1]) + \frac{\alpha_s^2}{(4\pi)^2} \beta_0 (u_0 \text{Im}[c_2] - c_0 \text{Im}[u_2]). \quad (60)$$

Because of the particular form of the amplitude for $B^- \rightarrow \pi^-\bar{K}^0$ shown in (38), $u_0 = c_0$ and $\text{Im}[u_i]$ differs from $\text{Im}[c_i]$ only by QCD penguin contributions. The result is that in (60) only the QCD penguins contribute to the asymmetry. Consequently this mode is insensitive to most of the model dependence in the BBNS framework.

It is important to note that our values of the CP asymmetries at $\mathcal{O}(\alpha_s)$ for $B^- \rightarrow \pi^0 K^-$ and $\bar{B}^0 \rightarrow \pi^+ K^-$ exhibit a much greater scale dependence than those of Beneke and Neubert

[64]. In our calculation of these asymmetries we keep the real parts of our amplitudes to only LO in α_s and it is the large scale dependence of these real parts that leads to the large scale dependence of our asymmetries. Beneke and Neubert on the other hand keep the real parts of their amplitudes to NLO and it is these higher order terms that result in their reduced scale dependence.

Because of their different focus, it is difficult to compare our results to those of Neubert and Pecjak [40]. These authors were primarily interested in estimating the size of non-perturbative corrections. Although they did calculate some leading perturbative corrections, they sought only to compare the size of these corrections to their estimate of the power corrections. As such, almost all of the parameters we chose to vary, including the renormalization scale, the LCDAs, as well as the form factors and decay constants, they simply held fixed, and no estimate of their induced uncertainties was made. They did calculate the CP asymmetries for the $\bar{B}^0 \rightarrow \pi^+ K^-$ and $B^- \rightarrow \pi^0 K^-$ decay modes. Their results are consistent with our own, to within our large uncertainties. Perhaps the most significant comparison concerns the size of the subleading corrections. They found, as we did, that the subleading corrections are substantial and can be almost as large as the leading order result.

Recently new measurements of the CP asymmetry in $\bar{B}^0 \rightarrow \pi^+ \pi^-$ were released by the BABAR [12] and BELLE [17] collaborations. In Figure 5 we show our results for the direct CP violation parameter $\mathcal{A}_{\pi\pi}$ defined in (42) as a function of the unitarity angle γ . The current experimental data for this quantity is

$$\begin{aligned} \text{BABAR}[12] : \mathcal{A}_{\pi\pi} &= 0.09 \pm 0.15(\text{stat}) \pm 0.04(\text{syst}) \\ \text{BELLE}[17] : \mathcal{A}_{\pi\pi} &= 0.56 \pm 0.12(\text{stat}) \pm 0.06(\text{syst}), \end{aligned} \tag{61}$$

The 1σ ranges for these measurements are superimposed in Figure 5.

Figure 5 shows that the calculated CP asymmetry has a large renormalization scale dependence at $\mathcal{O}(\alpha_s^2 \beta_0)$, which dominates the uncertainty in the prediction. Within the large error bars, the experimental results of BABAR are in fair agreement with these calculations, while the results of BELLE show a several σ deviation. Clearly, more work is required on both the experimental and theoretical sides before any definitive statement can be made about the success of the BBNS framework in this context. For instance, the contributions from power-suppressed annihilation diagrams should be included, as they are known to have a large effect on strong phases [24, 65].

V. CONCLUSIONS

In this paper we have calculated perturbative corrections to $B \rightarrow \pi\pi, \pi K$ decays up to $\mathcal{O}(\alpha_s^2 \beta_0)$ in the QCD factorization formalism, including ‘chirally enhanced’ power corrections but neglecting other corrections entering formally at $\mathcal{O}(\Lambda_{\text{QCD}}/m_b)$. We have included contributions from non-factorizable vertex diagrams, QCD penguin diagrams, and spectator

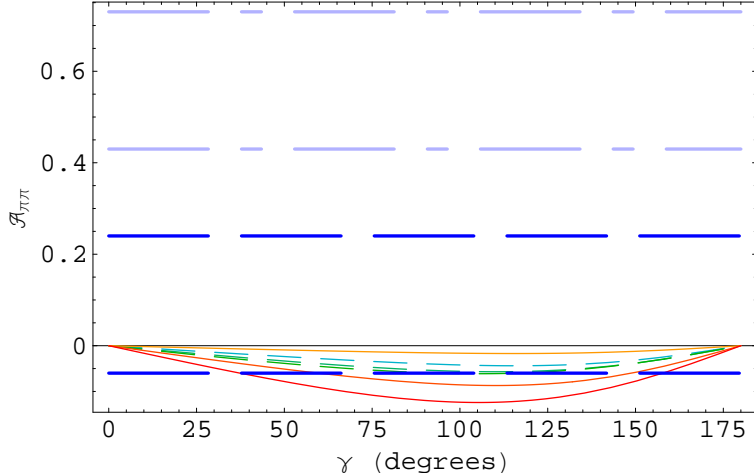


FIG. 5: The CP violating quantity $\mathcal{A}_{\pi\pi}$ as a function of the unitarity angle γ . The three short-dashed curves are the prediction at order $\mathcal{O}(\alpha_s)$, while the three solid curves include the perturbative corrections up to $\mathcal{O}(\alpha_s^2\beta_0)$. The lines in each set correspond to the three different renormalization scales $\mu = m_b/2$, $\mu = m_b$ and $\mu = 2m_b$. The heavy dashed and dot-dashed horizontal lines are the 1σ experimental uncertainties for BABAR and BELLE, respectively.

scattering diagrams. In all cases we have derived analytic expressions for the hard scattering kernels for general light-cone quark momentum distribution functions.

We have used these analytic results to study the direct CP asymmetries for a set of phenomenologically interesting decay modes. We focused on the behaviour of perturbation theory for this observable, and we estimated the uncertainties due to model dependent parameters.

For the direct CP asymmetries $\mathcal{A}_{\text{CP}}^{\text{Dir}}$, we found that contributions at $\mathcal{O}(\alpha_s^2\beta_0)$ are comparable to those at $\mathcal{O}(\alpha_s)$ for all the modes. This conclusion is in agreement with the results of [40], which indicated a large perturbative correction between one-loop and two-loop order in the large- β_0 limit. As well, we found a very strong dependence on the renormalization scale; in some cases the asymmetry varies over an order of magnitude.

For all modes, with the exception of $\mathcal{A}_{\text{CP}}^{\text{Dir}}(\pi^0\pi^0)$, the primary uncertainty at a given scale arises from uncertainty over the shape of the light cone momentum distribution amplitude. The uncertainties arising from form factors and spectator scattering model parameters are mode dependent and relatively small. The asymmetry $\mathcal{A}_{\text{CP}}^{\text{Dir}}(\pi^-\bar{K}^0)$ is particularly clean in the QCD factorization framework, having no dependence on form factors or spectator scattering parameters. Finally, we have examined the direct CP violation parameter $\mathcal{A}_{\pi\pi}$ in the $\bar{B}^0 \rightarrow \pi^+\pi^-$ decay mode and have found a large perturbative correction at $\mathcal{O}(\alpha_s^2\beta_0)$. The result agrees with the current experimental measurements, though the errors for both theory and experiment are large.

VI. ACKNOWLEDGMENTS

We would like to thank Michael Luke for discussions related to this project. This work is supported by the Natural Sciences and Engineering Research Council of Canada and by the Walter B. Sumner Foundation.

-
- [1] D. Cronin-Hennessy *et al.* [CLEO Collaboration], Phys. Rev. Lett. **85**, 515 (2000).
 - [2] D. M. Asner *et al.* [CLEO Collaboration], Phys. Rev. D **65**, 031103 (2002) [arXiv:hep-ex/0103040].
 - [3] S. Chen *et al.* [CLEO Collaboration], Phys. Rev. Lett. **85**, 525 (2000) [arXiv:hep-ex/0001009].
 - [4] B. Aubert *et al.* [BABAR Collaboration], Phys. Rev. Lett. **87**, 151802 (2001) [arXiv:hep-ex/0105061].
 - [5] B. Aubert *et al.* [BABAR Collaboration], Phys. Rev. D **65**, 051502 (2002) [arXiv:hep-ex/0110062].
 - [6] B. Aubert *et al.* [BABAR Collaboration], arXiv:hep-ex/0109007.
 - [7] B. Aubert *et al.* [BABAR Collaboration], arXiv:hep-ex/0206053.
 - [8] B. Aubert *et al.* [BABAR Collaboration], Phys. Rev. Lett. **89**, 281802 (2002) [arXiv:hep-ex/0207055].
 - [9] B. Aubert *et al.* [BABAR Collaboration], arXiv:hep-ex/0207063.
 - [10] B. Aubert *et al.* [BABAR Collaboration], arXiv:hep-ex/0207065.
 - [11] B. Aubert *et al.* [BABAR Collaboration], Phys. Rev. Lett. **93**, 231804 (2004) [arXiv:hep-ex/0408017].
 - [12] B. Aubert *et al.* [BaBar Collaboration], arXiv:hep-ex/0501071.
 - [13] K. Abe *et al.* [BELLE Collaboration], Phys. Rev. Lett. **87**, 101801 (2001) [arXiv:hep-ex/0104030].
 - [14] K. Abe *et al.* [BELLE Collaboration], Phys. Rev. D **64**, 071101 (2001) [arXiv:hep-ex/0106095].
 - [15] K. Abe *et al.* [Belle Collaboration], Phys. Rev. Lett. **93**, 021601 (2004) [arXiv:hep-ex/0401029].
 - [16] B. C. K. Casey *et al.* [Belle Collaboration], Phys. Rev. D **66**, 092002 (2002) [arXiv:hep-ex/0207090].
 - [17] K. Abe *et al.* [Belle Collaboration], arXiv:hep-ex/0502035.
 - [18] M. Bauer, B. Stech and M. Wirbel, Z. Phys. C **34**, 103 (1987).
 - [19] A. Deandrea, N. Di Bartolomeo, R. Gatto and G. Nardulli, Phys. Lett. B **318**, 549 (1993) [arXiv:hep-ph/9308210].
 - [20] M. Neubert, V. Rieckert, B. Stech and Q.P. Xu, in: *Heavy Flavours*, ed. A.J. Buras and M. Lindner (World Scientific, Singapore, 1992), pp. 286.
 - [21] M. Neubert and B. Stech, Adv. Ser. Direct. High Energy Phys. **15**, 294 (1998) [arXiv:hep-ph/9705292].

- [22] M. Beneke, G. Buchalla, M. Neubert and C. T. Sachrajda, Phys. Rev. Lett. **83**, 1914 (1999) [arXiv:hep-ph/9905312].
- [23] M. Beneke, G. Buchalla, M. Neubert and C. T. Sachrajda, Nucl. Phys. B **591**, 313 (2000) [arXiv:hep-ph/0006124].
- [24] M. Beneke, G. Buchalla, M. Neubert and C. T. Sachrajda, Nucl. Phys. B **606**, 245 (2001) [arXiv:hep-ph/0104110].
- [25] C. W. Bauer, D. Pirjol and I. W. Stewart, Phys. Rev. D **65**, 054022 (2002) [arXiv:hep-ph/0109045].
- [26] C. W. Bauer, D. Pirjol and I. W. Stewart, Phys. Rev. Lett. **87**, 201806 (2001) [arXiv:hep-ph/0107002].
- [27] C. W. Bauer, D. Pirjol and I. W. Stewart, Phys. Rev. D **67**, 071502 (2003) [arXiv:hep-ph/0211069].
- [28] J. Chay and C. Kim, Phys. Rev. D **65**, 114016 (2002) [arXiv:hep-ph/0201197].
- [29] J. g. Chay and C. Kim, arXiv:hep-ph/0205117.
- [30] M. Beneke, A. P. Chapovsky, M. Diehl and T. Feldmann, Nucl. Phys. B **643**, 431 (2002) [arXiv:hep-ph/0206152].
- [31] I. Z. Rothstein, Phys. Rev. D **70** (2004) 054024 [arXiv:hep-ph/0301240].
- [32] J. Chay and C. Kim, Nucl. Phys. B **680**, 302 (2004) [arXiv:hep-ph/0301262].
- [33] C. W. Bauer, D. Pirjol, I. Z. Rothstein and I. W. Stewart, Phys. Rev. D **70**, 054015 (2004) [arXiv:hep-ph/0401188].
- [34] T. Muta, A. Sugamoto, M. Z. Yang and Y. D. Yang, Phys. Rev. D **62**, 094020 (2000) [arXiv:hep-ph/0006022].
- [35] D. s. Du, D. s. Yang and G. h. Zhu, Phys. Lett. B **488**, 46 (2000) [arXiv:hep-ph/0005006].
- [36] D. s. Du, H. u. Gong, J. f. Sun, D. s. Yang and G. h. Zhu, Phys. Rev. D **65**, 074001 (2002) [arXiv:hep-ph/0108141].
- [37] K. G. Chetyrkin, A. L. Kataev and F. V. Tkachov, Phys. Lett. B **85**, 277 (1979);
M. Dine and J. R. Sapiirstein, Phys. Rev. Lett. **43**, 668 (1979);
W. Celmaster and R. J. Gonsalves, Phys. Rev. Lett. **44**, 560 (1980).
- [38] S. Narison and A. Pich, Phys. Lett. B **211**, 183 (1988);
E. Braaten, Phys. Rev. D **39**, 1458 (1989).
- [39] M. E. Luke, M. J. Savage and M. B. Wise, Phys. Lett. B **343**, 329 (1995) [arXiv:hep-ph/9409287];
T. van Ritbergen, Phys. Lett. B **454**, 353 (1999) [arXiv:hep-ph/9903226];
M. Steinhauser and T. Seidensticker, Phys. Lett. B **467**, 271 (1999) [arXiv:hep-ph/9909436].
- [40] M. Neubert and B. D. Pecjak, JHEP **0202**, 028 (2002) [arXiv:hep-ph/0202128].
- [41] C. N. Burrell and A. R. Williamson, Phys. Rev. D **64**, 034009 (2001) [arXiv:hep-ph/0101190].
- [42] T. Becher, M. Neubert and B. D. Pecjak, Nucl. Phys. B **619**, 538 (2001) [arXiv:hep-ph/0102219].

- [43] G. Buchalla, A. J. Buras and M. E. Lautenbacher, Rev. Mod. Phys. **68**, 1125 (1996) [arXiv:hep-ph/9512380].
- [44] A. V. Manohar and M. B. Wise, Phys. Lett. B **344**, 407 (1995) [arXiv:hep-ph/9406392].
- [45] V. M. Braun and I. E. Filyanov, Z. Phys. C **44**, 157 (1989) [Sov. J. Nucl. Phys. **50**, 511.1989 YAFIA,50,818 (1989)].
- [46] V. M. Braun and I. E. Filyanov, Z. Phys. C **48**, 239 (1990) [Sov. J. Nucl. Phys. **52**, 126 (1990)].
- [47] M. Beneke, Nucl. Phys. Proc. Suppl. **111**, 62 (2002) [arXiv:hep-ph/0202056].
- [48] G. P. Lepage and S. J. Brodsky, Phys. Rev. D **22**, 2157 (1980).
- [49] V. L. Chernyak and A. R. Zhitnitsky, Phys. Rept. **112**, 173 (1984).
- [50] S.V. Mikhailov and A.V. Radyushkin, JETP Lett. **43** 712 (1986); Sov. J. Nucl. Phys. **49** 494 (1989); Phys. Rev. D **45** (1992) 1754.
- [51] A. J. Buras and P. H. Weisz, Nucl. Phys. B **333**, 66 (1990).
- [52] M. Beneke, Phys. Rept. **317**, 1 (1999) [arXiv:hep-ph/9807443].
- [53] N. Pott, arXiv:hep-ph/9710503.
- [54] A. Ali, arXiv:hep-ph/0312303.
- [55] S. Eidelman *et al.* [Particle Data Group], Phys. Lett. B **592**, 1 (2004).
- [56] A. Khodjamirian, R. Ruckl, S. Weinzierl, C. W. Winhart and O. I. Yakovlev, Phys. Rev. D **62**, 114002 (2000) [arXiv:hep-ph/0001297].
- [57] P. Ball and R. Zwicky, JHEP **0110**, 019 (2001) [arXiv:hep-ph/0110115].
- [58] P. Ball and R. Zwicky, Phys. Rev. D **71**, 014015 (2005) [arXiv:hep-ph/0406232].
- [59] D. Melikhov and B. Stech, Phys. Rev. D **62**, 014006 (2000) [arXiv:hep-ph/0001113].
- [60] A. Abada, D. Becirevic, P. Boucaud, J. P. Leroy, V. Lubicz and F. Mescia, Nucl. Phys. B **619**, 565 (2001) [arXiv:hep-lat/0011065].
- [61] A. Abada, D. Becirevic, P. Boucaud, J. P. Leroy, V. Lubicz, G. Martinelli and F. Mescia, Nucl. Phys. Proc. Suppl. **83**, 268 (2000) [arXiv:hep-lat/9910021].
- [62] V. M. Braun and A. Lenz, Phys. Rev. D **70**, 074020 (2004) [arXiv:hep-ph/0407282].
- [63] Heavy Flavor Averaging Group (HFAG) data averages can be found at www.slac.stanford.edu/xorg/hfag/
- [64] M. Beneke and M. Neubert, Nucl. Phys. B **675**, 333 (2003) [arXiv:hep-ph/0308039].
- [65] Y. Y. Keum, H. n. Li and A. I. Sanda, Phys. Lett. B **504**, 6 (2001) [arXiv:hep-ph/0004004].